Updated Methodology for Permeability Modeling with Core Photos and Image Logs

Yevgeniy Zagayevskiy and Clayton V. Deutsch

The permeability modeling is a key element in construction of a geological model for petroleum reservoir characterization. It is unusual that core data is biased due to core handling, dilation, and preferential sampling. It is impossible to directly measure permeability by logging tools, and well test is hampered at bitumen rich oil sands reservoirs in northern Alberta. All these and other factors lead to limited permeability data. On the other hand, secondary highly correlated data can be used to infer permeability. There is a strong relationship between permeability and porosity, which is better-off sampled. Core photos and image logs (FMI) may even further improve permeability estimate. It is important to properly assimilate available auxiliary data that come from different sources and heterogeneity scales. Thus, by-facies multiscale permeability modeling workflow is proposed. The image data in addition to porosity-permeability relationship from core and petrophysical log data are used to supplement insufficient permeability measurements. The methodology consists of three main stages: micro, mini, and reservoir scale modeling, which is improved and simplified from legacy approaches. Monte Carlo simulation of porosity-permeability relationship is replaced with parametric regression fitting. Updated workflow properly assimilates and debias multiscale data. Vertical permeability is derived along with horizontal permeability, which is crucial for successful implementation of steam assisted gravity drainage (SAGD) heavy oil extraction technique. Permeability modeling of inclined heterolithic strata (IHS) facies at micro- and minimodeling scales is demonstrated with realistic case study that shows improvement of permeability.

Introduction

The primary objective of a petroleum geomodeling study is to build plausible geological model at appropriate scale. A geomodeling workflow may vary depending on purpose of the model and available data. In general, first, structural elements such as horizons, surfaces, and faults are modeled and then populated with representative petrophysical and geomechanical properties by-facies. Final geomodel should honor the data and is fed to flow simulation in order to describe future reservoir performance and predict production rate. Facies, porosity, and permeability are three most important petrophysical properties that determine lithology of a reservoir, volume of deposited oil, and how easily it can be produced, respectively. In northern Alberta oil sands reservoirs, vertical permeability is of the highest interest, because vertical flow is crucial in widely implemented steam assisted gravity drainage (SAGD) bitumen extraction technique (Butler, 1991). Vertical permeability defines communication between horizontal injector and producer, and establishes fluid flow paths from a reservoir to production wells.

Facies and porosity data come from core inspection, lab tests, and petrophysical surveys. Facies that are computed from a set of petrophysical logs using data classification or discrimination techniques are called electrofacies. Usually, log porosity measurements exceed log porosity data in number, since there are no missing log porosity measurements in logged wells. But core porosity data are missing from time to time, and especially in poor consolidated reservoirs. While core porosity data represent total porosity, log porosity measurements define effective values, which are used in modeling. Therefore, core porosity should be corrected against log porosity.

Permeability can be also measured at a core lab. But it is impossible to neither conduct a well test in a reservoir saturated with viscous oil, like bitumen in oil sands, nor measure permeability by petrophysical logs. Highly correlated porosity-permeability relationship and auxiliary data can be used to supplement insufficient permeability measurements and additionally constrain permeability models. In this paper, core images and image logs are used in addition to conventional set of data to build permeability models. Core data, petrophysical logs, and image data are sampled at different scales, which should be properly accounted for. Moreover, bias in core data and logs should be diminished.

Sequential multiscale modeling procedure of permeability conditional to porosity is not a novel idea. Permeability models are built within geostatistically stationary domains, which are represented by

facies in a geological setting. Therefore, facies model is constructed first. Then, more exhaustively sampled core data is used to build porosity models for each facies. Porosity-permeability transform from core data is used to co-simulate permeability field for each facies type (Deutsch, 2002). However, typically image data is not used to constrain permeability models.

The main reason for use of the core images (CIM) and image logs (FMI) in this study is that they represent smaller scale and, therefore, capture more detailed spatial information about configuration of heterogeneities in every facies. The core image is a color photo of a core sliced into half. The core photos are available for the most of the observation wells in northern Alberta oil fields. The core images are provided in JPG, TIF, or PDF formats. A sample of processed TIF core image is shown in Figure 3. The FMI abbreviation stands for the full bore formation micro image, which is an output of a tool developed by Schlumberger, and represents 360^0 wellbore-long measurement of the micro-resistivity of the borehole wall (Niven and Deutsch, 2011). The FMI data is provided in PDF or DLIS formats, a processed PDF sample of FMI is shown in Figure 4. The image data were provided by a TarCore lab for academic purposes at GeoConvention 2012, which is annually held in Calgary, Alberta.

There are some pros and cons associated with use of core images and FMI data, which are summarized in Table 1. The main advantage of using core images over FMI in by-facies porosity-permeability modeling is that the core photo is a direct physical measurement of rock structural patterns and texture of higher resolution with more details. The main advantage of FMI over core image is that the FMI is sampled along an entire well bore and represents 3D volume.

Table 1: Pros and cons of core images and FMI data usage in by-facies porosity-permeability modeling

Data	Pros	Cons
Core image	Direct visual representation of rock heterogeneities	Poor coverage - some intervals are missing (not available along entire wellbore) due to core sampling and specimen crumbling, possible depth shift
	High resolution with detailed structure and texture of the rock	2D sample of small size (about 8 cm width)
	Easy to identify facies, except bitumen rich intervals	Easy, but slow digitization from any available formats like JPG, TIF, and PDF (manual process)
FMI	Available along entire well bore	Indirect measurements of the rock heterogeneities (micro resistivity) and image artifacts due to pads sticking
	3D representation of the rock heterogeneities (bedding directions)	Lower resolution than in core images
	Easy and fast digitization from DLIS format (automatic process) using freeware DLIS2ASCII program by Schlumberger	Hard to identify and differentiate some facies, especially indurate sandstone and mudstone

This paper summarizes and improves existent multiscale modeling approaches of horizontal and vertical permeability in petroleum reservoirs, depositional environment of which is dominated by binary sand-shale sequences and shale clusts. Benefits of previous approaches are emphasized and improved. Shortcomings are addressed and resolved. Time consuming percolation modeling and subsequent Monte Carlo simulation (MCS) of porosity-permeability relationship are replaced with fast parametric regression fitting. The proposed methodology consists of three stages in order to account for varying data scales. First, micromodeling is performed, in which core images and/or image logs are digitized by-facies to account for small scale lamination in inclined heterolithic strata (IHS) facies and mud clusts in breccia facies deposited in tidally influenced reservoirs. Then, digitized images are combined with corrected core data to build porosity and permeability models at decimeter scale. Second, minimodeling is carried out to

incorporate petrophysical log data with results from previous stage into porosity-permeability models at meter scale. Finally, facies and porosity models are built at petroleum reservoir scale conditional to cleaned log data. Permeability model is co-simulated using porosity model, the porosity-permeability transform from minimodeling stage, and knowledge of permeability spatial structure.

This paper is organized as follows. First, a methodology for multiscale modeling of by-facies porosity-permeability relationships with core images and image logs is presented in details. Second, a case study is shown to understand benefits and drawbacks of use of core images and image logs. It is found that CIM- and FMI-based modeling results are similar with higher uncertainty imbedded into FMI data. Finally, conclusions are made, and future work is defined.

Workflow

The workflow presented in this paper is similar to previous by-facies multiscale permeability modeling approaches developed and promoted at the CCG. Number of peer-reviewed papers and conference articles are available. Early paper by McLennan et al. describes modeling of permeability at reservoir scale conditional to previously simulated porosity models and porosity-permeability relationship defined at the minimodeling scale (McLennan et al., 2006). Omitting important micromodeling scale, which may be supported by core images or image logs, leads to poor reproduction of V-shale. Several strong assumptions regarding minimodeling scale, like Gaussian nature of the porosity-permeability transform, are not supported by the data. Paper by Hosseini et al. attempts to resolve these issues by introducing missing micromodeling scale (Hosseini et al., 2008). Only core images are used to constrain the model at micromodeling scale. The results look promising, but the workflow is very tedious and only global porosity-permeability transform function can be derived, and no local permeability modeling tied to wells is performed due to missing intervals of core data. Knowing exact permeability values at the well locations should improve model quality. Therefore, use of image logs (FMI or HMI) is proposed by Niven and Deutsch to locally build permeability models along the wells and populate rest of 3D permeability models by geostatistical tools such as sequential Gaussian simulation (Niven and Deutsch, 2009). Measured micro resistivity is sensitive to presence of formation fluid around well bore and, thus, special attention should be made while digitizing water/gas saturated zones of FMI. An overview paper on multiscale permeability modeling can be found in (Deutsch, 2010) with some numerical examples in (Niven and Deutsch, 2011). Inherent advantages of these legacy multiscale porosity-permeability modeling approaches are construction of representative porosity-permeability relationship for each facies, debiasing core data, and cleaning log data. The bias is introduced by measurement errors, core handling, core dilation, preferential sampling, etc., and leads to elevated porosity and permeability values and missing measurements for low porosity tail (Figure 1).

The proposed workflow preserves the best of legacy approaches, and benefits in its robustness, maturity, and multiscale data honoring. Time consuming percolation modeling and subsequent Monte Carlo simulation (MCS) of porosity-permeability relationship are replaced with fast parametric regression fitting (Hosseini et al., 2008). The workflow consists of three main stages defined by various scales. First two stages are thoroughly explained with case study. Three stages are:

1- micromodeling stage
2- minimodeling stage
3- reservoir scale modeling stage

Introduction of three different modeling scales is motivated by different data support and target model scale. The data resolution and model grid specification used at each stage are summarized in Table 2. The output from antecedent stage is fed to subsequent stage. Note that this workflow is intended to build by-facies “global” by-facies porosity-permeability relationships for permeability modeling. The workflow can be slightly modified to locally co-simulate permeability along the well bore similar to approach by (Niven and Deutsch, 2009) and to omit regression fitting.

More detailed description of the multiscale modeling approach is provided below. High level flow chart for proposed permeability modeling is presented in Figure 2. Micromodeling stage is intended for establishment of by-facies parametric porosity-permeability relationships at core plug scale ~2.5 cm, which are used as transformation tables in minimodeling stage. Permeability is derived from cleaned log porosity in minimodeling stage at a core plug resolution and upscaled to ~1.0 m, which is about block size

of reservoir scale model. Resultant porosity-permeability transformation function for each facies in the form of a regression model is used at reservoir scale to build by-facies permeability models conditional to previously simulated porosity models and permeability spatial structure.

Table 2: Approximate size of micro-, mini-, and reservoir scale models and their blocks

Scale	Block Size ~	Model Size ~	Representative Data
Micromodeling scale	1 x 1 x 1 mm	1 x 1 x 1 dm	Core images and FMI
Minimodeling scale	1 x 1 x 1 dm	1 x 1 x 1 m	Core and log data
Reservoir model scale	1 x 1 x 1 m	10^n x 10^n x 10^n m, $n > 1$	Upscaled data above

The multiscale modeling starts with *data analysis*. Petrophysical porosity and V-shale, core porosity, core permeability, K_{ver}/K_{hor} permeability ratio and core V-shale are cleaned and assigned to associated facies from logs/core data according to lithology. Log porosity and V-shale data are cleaned by matching log facies data to core facies meauremnets and adjusting other petrophysical properties accordingly. Inflated core porosity data should be corrected by cleaned log data by matching mean values of two distributions. Simple multiplication of core porosity values by ratio of mean log porosity to mean core porosity is sufficient. A threshold may be applied to avoid unrealistically low values of corrected core porosity. Semivariogram models of by-facies cleaned log porosity and V-shale should be derived for later use in geomodeling.

The *micromodeling stage* consists of the following steps:

1- Select several by-facies representative core images/FMI data and digitize them as sand (0) or shale (1) units with fixed interval length. Lithological facies in the tidally influenced estuarine depositional systems of McMurray formation can be viewed as a binary mixture of good and bad quality rock units, like sand and shale. The difference between facies lies in the proportions, texture, structure, and continuity of sand-shale units. Some examples of typical estuarine facies are sand, breccia, sandy IHS (SIHS), muddy IHS (MIHS), mudstone, etc., which may be bioturbated or degraded by the time. This conceptual understanding of McMurray facies defines digitization aspect at micromodeling stage. V-shale and resistivity logs may be used in couple to assist in automatic digitization and reduce inherent effect of radioactive sand and formation water/gas on these log readings. GIMP or DLIS2ASCII freeware may be used to convert original image data formats like TIF and DLIS to ASCII.

2- Calculate elementary statistics for each digitized training image: mean and proportions.

3- Build anisotropic variogram model for each binary data set.

4- Create a 3D binary data set either by rotation or transposition for each digitized core image.

5- Build single realization of 3D binary indicator models (geo-blocks) using any categorical variable modeling technique for each digitized image interval. The models will consist of clean sand and clean shale units at pixel resolution. Multiple-point statistics (MPS) may be preferred over sequential indicator simulation (SIS). Dipping is important feature of laminated facies like IHS and should be preserved in 3D binary models.

6- Populate binary indicator models with representative clean sand and clean shale porosity and permeability values. Corrected sand and shale facies distributions are used as to derive these representative values. Corrected core porosity is no longer associated with total porosity, but rather with effective porosity. Populated clean sand permeability is further adjusted to local V-shale content.

7- Find effective values of petrophysical properties by upscaling populated models from pixel scale to scale of a micromodel, which is about core plug scale. Use arithmetic averaging for porosity upscaling, and steady-state single-phase flow simulator for permeability upscaling.

8- Combine upscaled values from all images together for each facies, and fit statistical regression models to each combined upscaled porosity-horizontal permeability relationship. Assume constant K_{ver}/K_{hor} permeability ratio from core data, which will be used as input to minimodeling stage.

The procedure of *minimodeling stage* is as follows:

1- Construct by-facies *N* realizations of porosity models at core plug resolution using variograms of cleaned log porosity data and their histograms as reference distributions. SGS may be a good simulation tool.
2- Co-simulate with cloud transformation (p-field simulation) *N* realizations of K_{hor} models for each facies conditional to *N* porosity minimodels from step 1 using porosity-horizontal permeability regression model from micromodeling stage and V-shale variogram model to generate probability field. It is believed that V-shale variogram is an adequate substitute for K_{hor} variogram, because experimental variogram range of V-shale is less than variogram range of porosity data. Difference in variogram ranges is dictated by larger spatial variability in permeability field in comparison with porosity. Assume K_{ver} to be a product of simulated K_{hor} and constant permeability ratio from core data.
3- Upscale porosity and permeability from core plug scale to minimodeling scale (~1.0 m) similar as it is done in the micromodeling stage.
4- Fit statistical regression models by-facies to upscaled porosity-K_{hor} and K_{hor}-K_{ver} values and use these models later on in reservoir scale modeling. Note that K_{ver}/K_{hor}-horizontal permeability curve is obtained from K_{hor}-K_{ver} fit regression model. Both deterministic and stochastic regression modeling options are available.

The *reservoir scale modeling* is a final stage in porosity and permeability modeling. The output of this stage should be used for reservoir forecasting by full field simulation. Reservoir scale modeling is straightforward and, thus, not included into the case study. The procedure is described below and similar to minimodeling.

1- Build *N* realizations of facies model at the reservoir scale using corrected core and cleaned log data. Again, MPS may be preferred over SIS.
2- Construct *N* realizations of porosity models for each facies using cleaned log data.
3- Simulate by-facies horizontal permeability K_{hor} by cloud transformation using constructed porosity models from step 2, statistical porosity-horizontal pemreability regression models from minimodeling, and V-shale variogram models as substitute for horizontal permeability variogram models.
4- Simulate by-facies K_{ver}/K_{hor} ratio using core data and V-shale variogram model and derive vertical permeability from product of K_{hor} and K_{ver}/K_{hor}. Or simulate for each facies K_{ver} by cloud transformation using constructed K_{hor} models from step 3, statistical $K_{hor} - K_{ver}$ regression models from minimodeling stage, and V-shale variogram models as substitute for vertical permeability variogram models.
5- Use derived petrophysical properties in flow simulation for reservoir forecasting

A case study on multiscale porosity and permeability modeling for IHS facies is shown below. Final core image- and image log-based permeability models are constructed separately to compare informational value of each data type. Role of the regression models is emphasized.

Case Study

The goal of this case study is to show how proposed permeability modeling methodology can be used with core image and image log data to build representative porosity-horizontal permeability and horizontal permeability-vertical permeability relationships at micro- and minimodeling scales. These relationships are used to derive final porosity and permeability models at reservoir scale. Both CIM and FMI are found to equally well improve the permeability estimate with higher variability present in FMI-based models, which is due to larger sampling volumes and lower data resolution. The FORTRAN programs used in this work can be enquired from the authors.

The image data are provided by TarCore lab. All other modeling parameters are adapted from (Deutsch, 2010) and assumed to be corrected and cleaned. Therefore, no data analysis is necessary. Scatter plot of typical uncorrected core porosity and horizontal permeability data of IHS facies is shown in Figure 1. It is believed that mean porosity value of 0.326 is too high for IHS and is inflated due to several previously discussed factors like core dilation. There are no enough data at lower porosity tail either. The measured K_{ver}/K_{hor} ratio is assumed to be higher than 0.7 and shown in Figure 16 in magenta. The task is

to derive representative porosity-permeability relationship for IHS facies at reservoir modeling scale by correcting core porosity values, extrapolating porosity-permeability function for low values, and properly accounting for scale change. Vertical permeability should be also derived.

Micromodeling stage starts with IHS digitization of bioturbated CIM and low resolution FMI. Since limited number of data is provided by TarCore, only one core image and one image log are selected for permeability modeling. Both image data represent different IHS intervals sampled from different wells. The CIM is digitized using global threshold. Local threshold is used for FMI digitization. Sand (0 or blue) and shale (1 or red) proportions are computed. Experimental variograms for horizontal (red) and vertical (blue) directions are derived from the CIM and FMI image data. Anisotropic variogram models are fit to both experimental variograms. Image analysis results are shown in Figure 3 for CIM and in Figure 4 for FMI. By looking at the proportions and digitized images, it is argued that CIM image data represents muddy IHS, and FMI image data is a measurement of sandy IHS. Since digitized core image is 2D binary data, rotation or transposition of the image data is necessary to generate 3D data set. Previous studies have shown that transposition creates spatial artifacts, e.g. variogram is not reproduced, and excessive rotation of 2D planes makes important dipping direction smooth. Therefore, core image data is rotated only once to recreate 3D binary data (Figure 5). The SIS is used to generate 3D binary models from both CIM and FMI (Figure 5). The resolution of the data and model grids are tabulated in Table 3. Well bore diameter of 159.0 mm is assumed.

Table 3: Model grid definition at various scales for CIM and FMI. CIM data resolution is 0.625 x 0.286 mm^2, and FMI data resolution is 2.080 x 2.500 mm^2.

Model Scale	Image	Model Resolution, mm	Model Grid, # blocks	Model Size, mm
Pixel scale	Core image	0.625 x 0.625 x 0.286	80 x 80 x 700	50.00 x 50.00 x 200.00
	Image log	2.080 x 2.080 x 2.500	78 x 78 x 375	162.24 x 162.24 x 937.50
Micromodeling scale	Core image	25.00 x 25.00 x 28.57	2 x 2 x 7	50.00 x 50.00 x 200.00
	Image log	27.04 x 27.04 x 37.50	6 x 6 x 25	162.24 x 162.24 x 937.50
Core plug scale	Core image	25.0 x 25.0 x 25.0	40 x 40 x 40	1000.0 x 1000.0 x 1000.0
	Image log	25.0 x 25.0 x 25.0	40 x 40 x 40	1000.0 x 1000.0 x 1000.0
Minimodeling scale	Core image	1000.0 x 1000.0 x 1000.0	1 x 1 x 1	1000.0 x 1000.0 x 1000.0
	Image log	1000.0 x 1000.0 x 1000.0	1 x 1 x 1	1000.0 x 1000.0 x 1000.0

Next step is the population of 3D binary models with representative statistics of clean sand and clean shale distribution parameters. If distribution of sand facies porosity and permeability is examined closer, a mixture of clean sand and contaminants can be distinguished due to sampling and measurement errors. Figure 6 contains typical histogram of corrected core porosity of sand facies in black. Such distribution can be viewed as combination of the normal distribution of clean sand in red and normal distribution of impurities and contaminants in green. Similar behavior is observed on normal probability plot (Figure 6). Straight red line represents normal distribution of clean pure sand with mean at 50% probability. 95% probability interval centered at the mean represents ± two standard deviations of the normal distribution. Thus, distribution parameters (mean and standard deviation) of clean sand unit are determined by drawing straight lines from 2.5%, 50%, and 97.5% probability values until they cross the red line, and picking appropriate porosity values (Figure 6, and Eqs. (1) and (2)). It happens that mean and standard deviation of clean sand porosity are 0.35 and 0.01, and 3.699 and 0.2 for horizontal permeability in log10 units. It is important to keep in mind that distribution of permeability is not normal in original units, but quite Gaussian in logarithmic units. Mean of K_{ver}/K_{hor} permeability ratio for IHS facies is assumed to be 0.8, estimate of which comes from the core data. Parameters of clean shale porosity and log10 permeability are assumed to be constant and equal to 0.01 and -2.0, respectively.

$$E\left[\phi_{sand\ sequence}\right] = \phi_{p=50\%} \tag{1}$$

$$VAR\left[\phi_{sand\ sequence}\right]=\left(\frac{\phi_{p=97.5\%}-\phi_{p=2.5\%}}{4}\right)^2 \quad (2)$$

In reality, however, permeability values in sandy parts of IHS do not always precisely follow distribution of clean sand permeability. Permeability of clean sand intervals within IHS facies also depends on local V-shale and is worse for higher shale content. Thus, permeability is corrected according to Eq. (3) to take into account influence of local V-shale. Permeability value at 25% of V-shale can be found from regression line on local core V-shale – horizontal permeability scatter plot (Figure 6).

$$\log\left(K_{hor,sand\ unit}(V_{shale})\right)=\log(K_{hor,clean\ sand})-4\cdot V_{shale}\cdot\left[\log(K_{hor,clean\ sand})-\left(\log K_{hor,sand}(V_{shale}=0.25)\right)\right] \quad (3)$$

Populated with porosity and permeability values 3D binary models and associated histograms for CIM- and FMI-based results are shown in Figure 7 and Figure 8, respectively. Since binary models are different for CIM and FMI, resulting populated porosity and permeability models also differ from each other. The conceptual statistics of IHS facies is preserved, which are depicted on the histograms. Mean porosity and permeability are smaller for CIM-based model in comparison with FMI-based model. This is obvious outcome, since V-shale is higher for CIM, and less for FMI. Local V-shale values are found by smoothing sand-shale binary models within ~10.0 cm window interval in all directions.

Upscaling of petrophysical properties from pixel scale to micromodeling scale is the next step. Input and output grid parameters of models are listed in Table 3. Note that model volume does not change, only block sizes increase from pixel to micromodeling scale. Arithmetic average upscaling is used for porosity and V-shale attributes, and single-phase steady state flow-based upscaling is used for permeability. In flow-based upscaling, the total Darcy's flow rate should be equal for upscaled and original models. This constrain is used to come up to effective permeability values. Upscaled results are shown in Figure 9 and Figure 10. Mean values of porosity and permeability are preserved during upscaling as it should be in accordance with dispersion variance theory. Histograms become smoother and less variable.

Final step of micromodeling stage is the fitting of porosity-horizontal permeability relationship with stochastic regression model. Ideally, upscaled results from conditioning images would be merged together (separately several CIM and FMI) to have larger representative set of data. But only one CIM image and one FMI image are available for this study. Mean of the bivariate distribution and standard deviation of residuals, which are found by subtraction of porosity values from their local means, are modeled independently. Regression equation for the mean is shown in Eq. (4) (Deutsch, 2010). Residuals are assumed to follow normal distribution with homoscedastic characteristic. Polynomial equation of third order is selected to fit the standard deviation as shown in Eq. (5). Conditional variance of residuals $\varepsilon(\phi) = \log_{10}(K^*_{hor}|\phi) - \log_{10}(K_{hor}|\phi)$ is computed as a variance of values falling inside a window of 0.1 size centered at specific porosity ϕ. The least squared error (LSE) optimization problem is solved to find regression coefficients for both models. The minimum value of sum of squared differences between model estimates and true values (data) is sought.

$$\log_{10}\left(K^*_{hor}\right)=\log_{10}(K_{hor,\min})+a_1\cdot\phi+a_2\cdot(1.0-e^{-3\cdot\phi/\phi_c}) \quad (4)$$

$$\sqrt{VAR\left[\log_{10}\left(K^*_{hor}|\phi\right)-\log_{10}(K_{hor}|\phi)\right]}=b_1+b_2\cdot\phi+b_3\cdot\phi^2+b_4\cdot\phi^3 \quad (5)$$

where K^*_{hor} is the estimate of horizontal permeability; $K_{hor,min}$ is the minimum horizontal permeability, or horizontal permeability of clean shale facies, which is 0.01 mD in our case; ϕ_c is the critical value of porosity, after which permeability does not change very much. In this case critical porosity equals to 0.30; a_1 and a_2 are the regression coefficients of mean porosity-horizontal permeability model; and b_1, b_2, b_3, and b_4 are the regression coefficients of residual variance model.

The LSE optimization problem for derivation of regression coefficients may be defined as shown in Eq. (6). The resultant equations for regression coefficients of mean and residual standard deviation models are shown in Eqs. (7) – (9).

$$\min[LSE] = \min\left[\sum_{i=1}^{n}\left(V_i^* - V_i\right)^2\right] \Rightarrow \frac{\partial LSE}{\partial a_j} = 0, \quad j = 1,...,m \tag{6}$$

$$a_1 = \frac{\sum_{i=1}^{n}\log_{10}(K_{hor})\cdot\phi - \log_{10}(K_{hor,\min})\cdot\sum_{i=1}^{n}\phi - \frac{\sum_{i=1}^{n}\phi\cdot(1.0-e^{-3\phi/\phi_c})\cdot\left(\sum_{i=1}^{n}\log_{10}(K_{hor})\cdot(1.0-e^{-3\phi/\phi_c}) - \log_{10}(K_{hor,\min})\cdot\sum_{i=1}^{n}(1.0-e^{-3\phi/\phi_c})\right)}{\sum_{i=1}^{n}(1.0-e^{-3\phi/\phi_c})^2}}{\sum_{i=1}^{n}\phi^2 - \frac{\left(\sum_{i=1}^{n}\phi\cdot(1.0-e^{-3\phi/\phi_c})\right)^2}{\sum_{i=1}^{n}(1.0-e^{-3\phi/\phi_c})^2}} \tag{7}$$

$$a_2 = \frac{\sum_{i=1}^{n}\log_{10}(K_{hor})\cdot(1.0-e^{-3\phi/\phi_c}) - \log_{10}(K_{hor,\min})\cdot\sum_{i=1}^{n}(1.0-e^{-3\phi/\phi_c})}{\sum_{i=1}^{n}(1.0-e^{-3\phi/\phi_c})^2} - a_1\frac{\sum_{i=1}^{n}\phi\cdot(1.0-e^{-3\phi/\phi_c})}{\sum_{i=1}^{n}(1.0-e^{-3\phi/\phi_c})^2} \tag{8}$$

$$\begin{bmatrix} b_1 \\ b_2 \\ b_3 \\ b_4 \end{bmatrix} = \begin{bmatrix} n & \sum_{i=1}^{n}\phi & \sum_{i=1}^{n}\phi^2 & \sum_{i=1}^{n}\phi^3 \\ \sum_{i=1}^{n}\phi & \sum_{i=1}^{n}\phi^2 & \sum_{i=1}^{n}\phi^3 & \sum_{i=1}^{n}\phi^4 \\ \sum_{i=1}^{n}\phi^2 & \sum_{i=1}^{n}\phi^3 & \sum_{i=1}^{n}\phi^4 & \sum_{i=1}^{n}\phi^5 \\ \sum_{i=1}^{n}\phi^3 & \sum_{i=1}^{n}\phi^4 & \sum_{i=1}^{n}\phi^5 & \sum_{i=1}^{n}\phi^6 \end{bmatrix}^{-1} \cdot \begin{bmatrix} \sum_{i=1}^{n}\sqrt{VAR[\log_{10}(K_{hor}\mid\phi)]} \\ \sum_{i=1}^{n}\phi\cdot\sqrt{VAR[\log_{10}(K_{hor}\mid\phi)]} \\ \sum_{i=1}^{n}\phi^2\cdot\sqrt{VAR[\log_{10}(K_{hor}\mid\phi)]} \\ \sum_{i=1}^{n}\phi^3\cdot\sqrt{VAR[\log_{10}(K_{hor}\mid\phi)]} \end{bmatrix} \tag{9}$$

where V is the variable of investigation; V^* is its estimate; a_j is the j^{th} regression coefficient; m is the number of regression coefficients for specific model; and n is the number of data.

Resulting linear regression models of porosity-horizontal permeability relationships with one and two standard deviation intervals are shown in Figure 11 for core photo and FMI. On average, regression models look alike for CIM and FMI, with larger uncertainty in FMI. This is reasonable result, since resolution of FMI is worse and smoothens important geological features. These regresion models are used as transformation functions in minimodeling stage. Regression coefficients are tabulated in Table 4.

Minimodeling stage consists of four main steps. First, N = 89 realizations of porosity is simulated unconditionally to the local data with variogram model from cleaned log porosity data. The shape of distribution is conditioned to the shape of cleaned log porosity data. The size of the models is chosen to be 1.0 m^3 with a resolution of 2.5 cm^3, which is about a core plug size (Table 3). Histograms of reference data and generated porosity are shown in Figure 12. A 3D view of single porosity realization and anisotropic porosity variogram model are presented on the same figure. Some lamination is observed in 3D porosity model. Note that same resulting porosity realizations are used in next step for CIM- and FMI-based permeability modeling.

Second step is the co-simulation of horizontal permeability conditional to porosity models using porosity-horizontal permeability transform function from micromodeling stage and permeability spatial structure. The transformation table is obtained from regression models (4) and (5) by Monte Carlo simulation drawing. P-field simulation is used to co-simulate horizontal permeability. Probability field is generated by unconditional SGS with variogram model from cleaned log V-shale data that are deemed to be plausible substitute for spatial structure of horizontal permeability. Single realization of horizontal permeability model for CIM- and FMI-based approaches is shown in Figure 13 and Figure 14, respectively.

Lamination features of IHS facies are observed in the permeability models. These models honor porosity data and transformation functions from micromodeling stage. Mean of horizontal permeability of CIM-based models is smaller than of FMI-based results due to higher shale content in conditioning CIM image, which is preserved through the transform function.

Third step is to upscale models from core plug scale to minimodeling scale. Model grid definition is shown in Table 3. Here, single realization of core plug scale model is upscaled to a minimodel that consists of a single block. The mean of K_{ver}/K_{hor} permeability ratio is assumed to be 0.8. Upscaling is carried out in a similar way to what is done at micromodeling stage: porosity is upscaled arithmetically, and tensor-based upscaling is used for permeability upscaling. Histograms of upscaled porosity and permeability are shown in Figure 15. Since porosity models used for the CIM and FMI-based modeling are the same, the upscaled results are unique as well. As expected, means of horizontal and vertical permeability are smaller for CIM than for FMI. Vertical permeability is less than horizontal permeability as defined in input parameters.

The last step is to fit regression models to porosity-permeability and horizontal-vertical permeability relationships. The $K_{hor} - K_{ver}/K_{hor}$ model is just simply derived from the $K_{ver} - K_{hor}$ regression model by dividing K_{ver} to K_{hor} values. Porosity-permeability regression model is similar to one used at the micromodeling stage (Eqs. (4) and (5)). Horizontal-vertical permeability relationship is fit slightly different – with second order polynomial function as shown in Eq. (10). Regression model for standard deviation of residuals are found similar to Eq. (5), and is expressed in Eq. (11). Again, the regression coefficients are derived by minimizing LSE (Eqs. (9) and (12)) and tabulated in Table 4. Obtained regression models for mean and ± one and two standard deviations for CIM- and FMI-based results are shown in Figure 16 with corrected core data. Note that permeability values with K_{ver}/K_{hor} permeability ratio R lower than 0.3 and higher than 1.0 are not used to constrain the regression model. These final regression models are used to simulate horizontal and vertical permeability values at reservoir scale conditional to porosity models derived from cleaned log data using co-simulation technique similar to one used in minimodeling stage (p-field simulation).

The reservoir scale modeling is not touched in this paper and is considered to be straightforward.

$$\log_{10}(K^{*}_{ver}) = \log_{10}(K_{hor,\min} \cdot R) + c_1 \cdot \left[\log_{10}(K_{hor}) - \log_{10}(K_{hor,\min})\right] + c_2 \cdot \left[\log_{10}(K_{hor}) - \log_{10}(K_{hor,\min})\right]^2 \quad (10)$$

$$\sqrt{VAR\left[\log_{10}\left(K^{*}_{ver} \mid K_{hor}\right) - \log_{10}(K_{ver} \mid K_{hor})\right]} = d_1 + d_2 \cdot \log_{10}(K_{hor}) + d_3 \cdot \log_{10}(K_{hor})^2 + d_4 \cdot \log_{10}(K_{hor})^3 \quad (11)$$

$$\begin{bmatrix} c_1 \\ c_2 \end{bmatrix} = \begin{bmatrix} \sum_{i=1}^{N} \log_{10}(K_{hor})^2 & \sum_{i=1}^{N} \log_{10}(K_{hor})^3 \\ \sum_{i=1}^{N} \log_{10}(K_{hor})^3 & \sum_{i=1}^{N} \log_{10}(K_{hor})^4 \end{bmatrix}^{-1} \cdot \begin{bmatrix} \sum_{i=1}^{N} \log_{10}(K_{hor}) \cdot \log_{10}(K_{ver}) \\ \sum_{i=1}^{N} \log_{10}(K_{hor})^2 \cdot \log_{10}(K_{ver}) \end{bmatrix} \quad (12)$$

Table 4: Regression model coefficients for porosity-horizontal permeability and horizontal-vertical permeability relationships fit at different modeling scales. $K_{hor,min}$ = 0.01 mD, and R = 0.8.

Model Scale	Image Data	Porosity-Horizontal Permeability Regression Model Coefficients	Horizontal Permeability-Vertical Permeability Regression Model Coefficients
Micro-modeling scale	Core image	a_1 = 5.49, a_2 = 3.69 b_1 = 0.24, b_2 = -0.47, b_3 = 1.41, b_4 = -1.53	-
	Image log	a_1 = 0.14, a_2 = 5.26 b_1 = 0.74, b_2 = -3.31, b_3 = 8.30, b_4 = -4.75	-
Mini-modeling scale	Core image	a_1 = 3.51, a_2 = 4.26 b_1 = 0.16, b_2 = 0.02, b_3 = -0.09, b_4 = 0.06	c_1 = 0.51, c_2 = 0.10 d_1 = 0.16, d_2 = 0.00, d_3 = 0.00, d_4 = 0.00
	Image log	a_1 = -2.62, a_2 = 6.30 b_1 = 0.30, b_2 = -0.25, b_3 = 3.03, b_4 = -7.25	c_1 = 0.79, c_2 = 0.04 d_1 = 0.17, d_2 = -0.01, d_3 = 0.00, d_4 = 0.00

Conclusions

The multiscale workflow for by-facies porosity, horizontal and vertical permeability modeling has been presented with illustrative realistic case study. The methodology consists of three stages due to multiscale nature of the data. Multiscale data are used to support the models at various reservoir heterogeneity scales. The stages are micromodeling, minimodeling, and reservoir scale modeling. At micromodeling stage, core images and image logs condition models at pixel scale and enable to reproduce small scale variability of lithological facies in the models. Corrected core porosity data is used to populate binary models with representative statistics. It is found that both CIM and FMI lead to the similar results with higher uncertainty in image log-based models because of associated lower image data resolution. At the minimodeling stage, by-facies porosity-horizontal permeability regression models from previous stage are used along with cleaned log data to build porosity-horizontal permeability and horizontal-vertical permeability bivariate models at meter scale, which is about a block size of petroleum reservoir model used for flow simulation. Results from minimodeling are used to co-simulate insufficiently sampled permeability. Permeability models are conditioned to well-defined porosity models from cleaned log data. Variogram models of V-shale are used to characterize permeability spatial structure and are deemed to be fair substitute. Bivariate relationships are summarized by regression models in deterministic or stochastic fashion. Final porosity and permeability models are delivered at reservoir scale suitable for flow simulation.

The methodology is deemed to be well-established with ability to deliver plausible and statistically sound results. The methodology is suitable for modeling of effective petrophysical properties of tidal influenced estuarine depositional systems in McMurray and other similar formations. It is able to debias core data and extrapolate missing lower tail of the distribution.

As for the future work, following tasks are proposed:

1- Derived by-facies porosity-permeability relationships may be validated by calibrating to production data or other observations.
2- Exhaustively available FMI data can be used for local modeling of permeability along the wells. Such local approach has an advantage over described approach. There is no need to subdivide data into the facies.
3- Influence of formation water and gas, and dipping directions on permeability modeling should be examined.

References

Butler, R. 1991. Thermal Recovery of Oil and Bitumen. Englewood Cliffs, Prentice Hall, 528 p.

Deutsch, CV, Journel, AG. 1998. GSLIB: Geostatistical Software Library and User's Guide: 2nd edition. New York: Oxford University Press, 369 p.

Deutsch, CV. 2002. Geostatistical Reservoir Modeling. New York: Oxford University Press, 376 p.

Deutsch, CV. 2010. Estimation of Vertical Permeability in the McMurray Formation. *Journal of Canadian Petroleum Technology*, 49(12), 1 – 8.

Hosseini, AH, Leuangthong, O, Deutsch, CV. 2008. An Integrated Approach to Permeability Modeling Using Micro-Models. *SPE International Thermal Operations and Heavy Oil Symposium*, Calgary, Alberta.

McLennan, JA, Deutsch, CV, Garner, D, Wheeler, TJ, Richy, J-F, Mus, E. 2006. Permeability Modeling for the SAGD Process Using Minimodels. *SPE Annual Technical Conference and Exhibition*, San Antonio, Texas.

Niven, EB, Deutsch, CV. 2009. Calculating Permeability from FMI Images in Oil Sand Deposits. *Centre for Computational Geostatistics*: Report 11, 212-1 – 212-6.

Niven, EB, Deutsch, CV. 2011. Permeability from Core Photos and Images. *Centre for Computational Geostatistics*: Guidebook Series 12, 45 p.

Srivastava, RM. 1992. Reservoir Characterization with Probability Field Simulation, *67th Annual Technical Conference and Exhibition of the SPE*, 927 – 938.

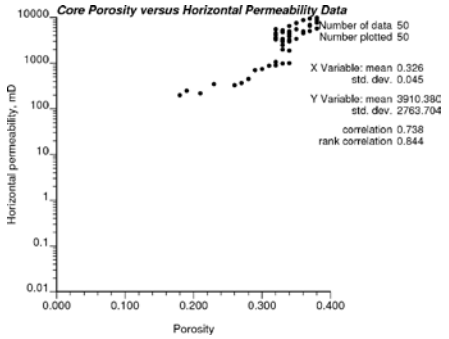

Figure 1: Typical core porosity-horizontal permeability data for laminated facies. It is believed that due to some factors, such as core dilation and preferential sampling, the data is biased and mostly represents good quality part of the facies. Therefore, the data should be corrected before integration into the geological model.

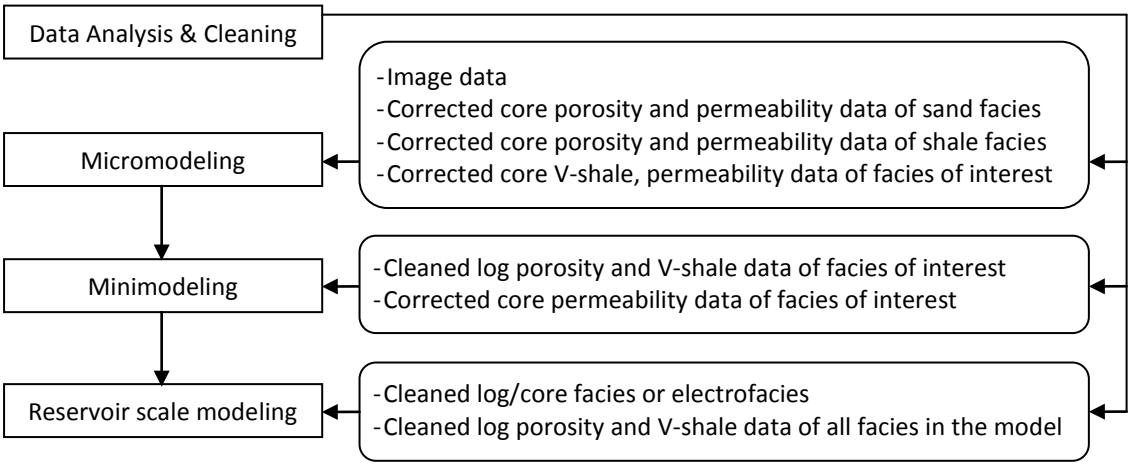

Figure 2: High level flow chart of the by-facies porosity and permeability modeling

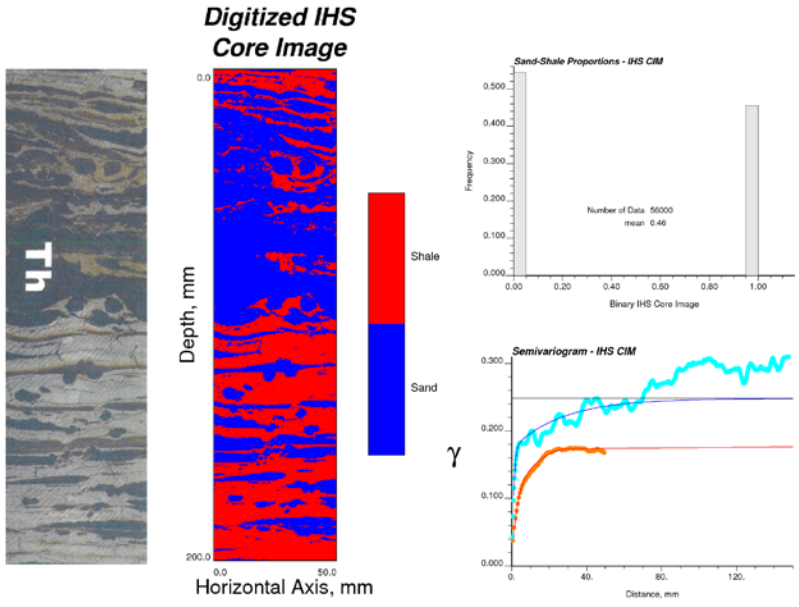

Figure 3: Micromodeling steps 1, 2, and 3: core photo digitization of IHS facies (from TarCore lab handout)

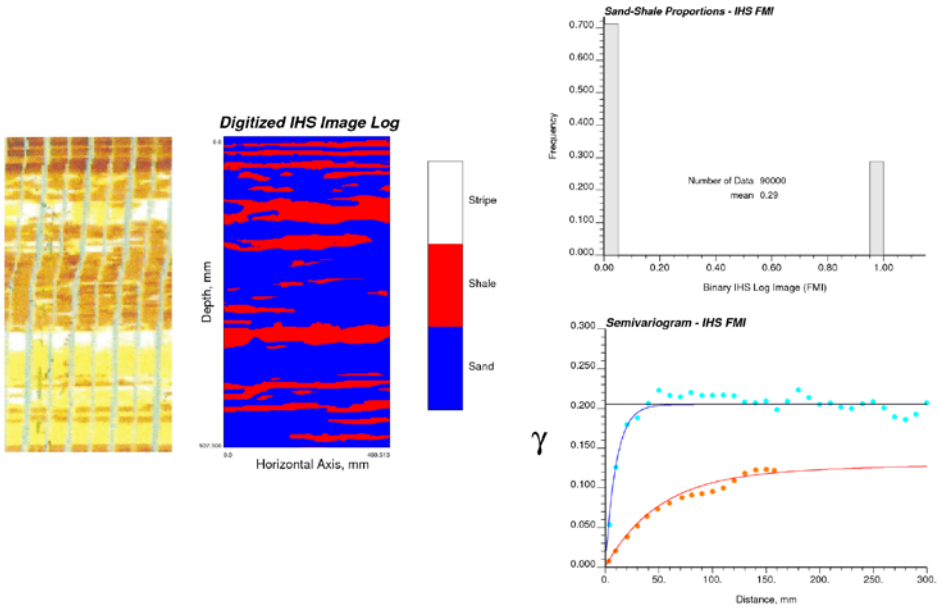

Figure 4: Micromodeling steps 1, 2, and 3: image log digitization of IHS facies (from TarCore lab handout)

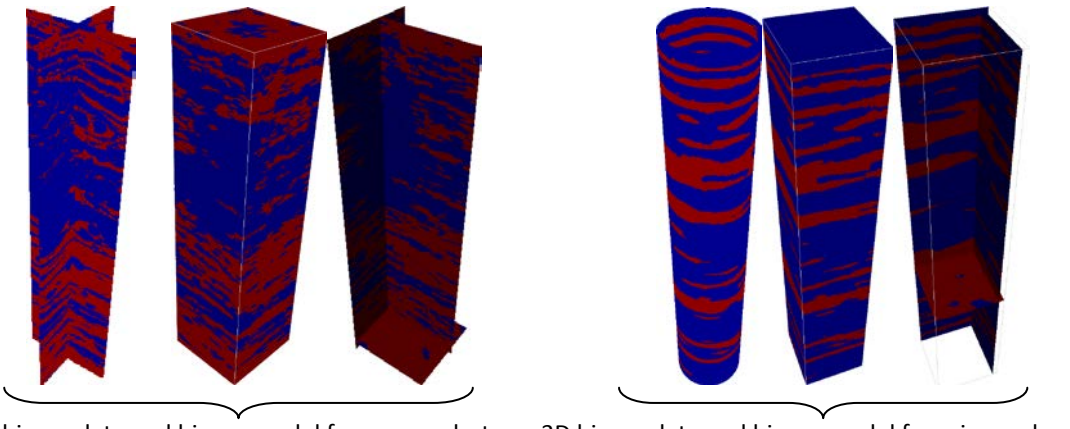

Figure 5: Micromodeling steps 4 and 5: building a binary sand-shale IHS model from 3D data

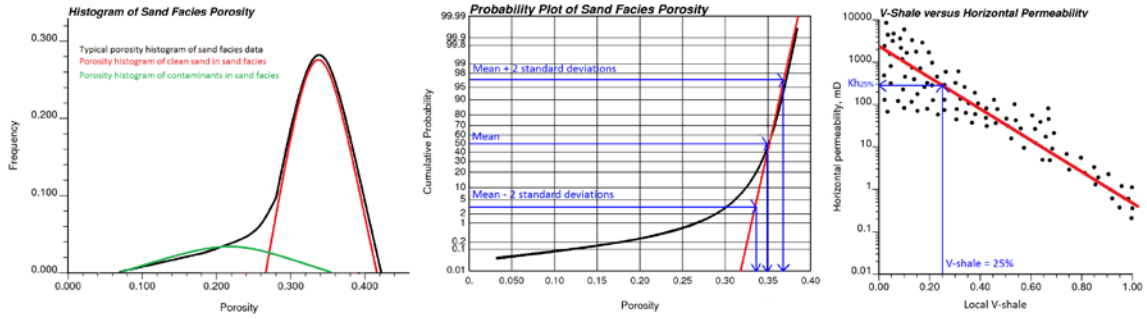

Figure 6: Micromodeling step 6: choosing representative distribution parameters of clean sand porosity and horizontal permeability from corrected core data of sand facies. Schematic representation of the process is provided.

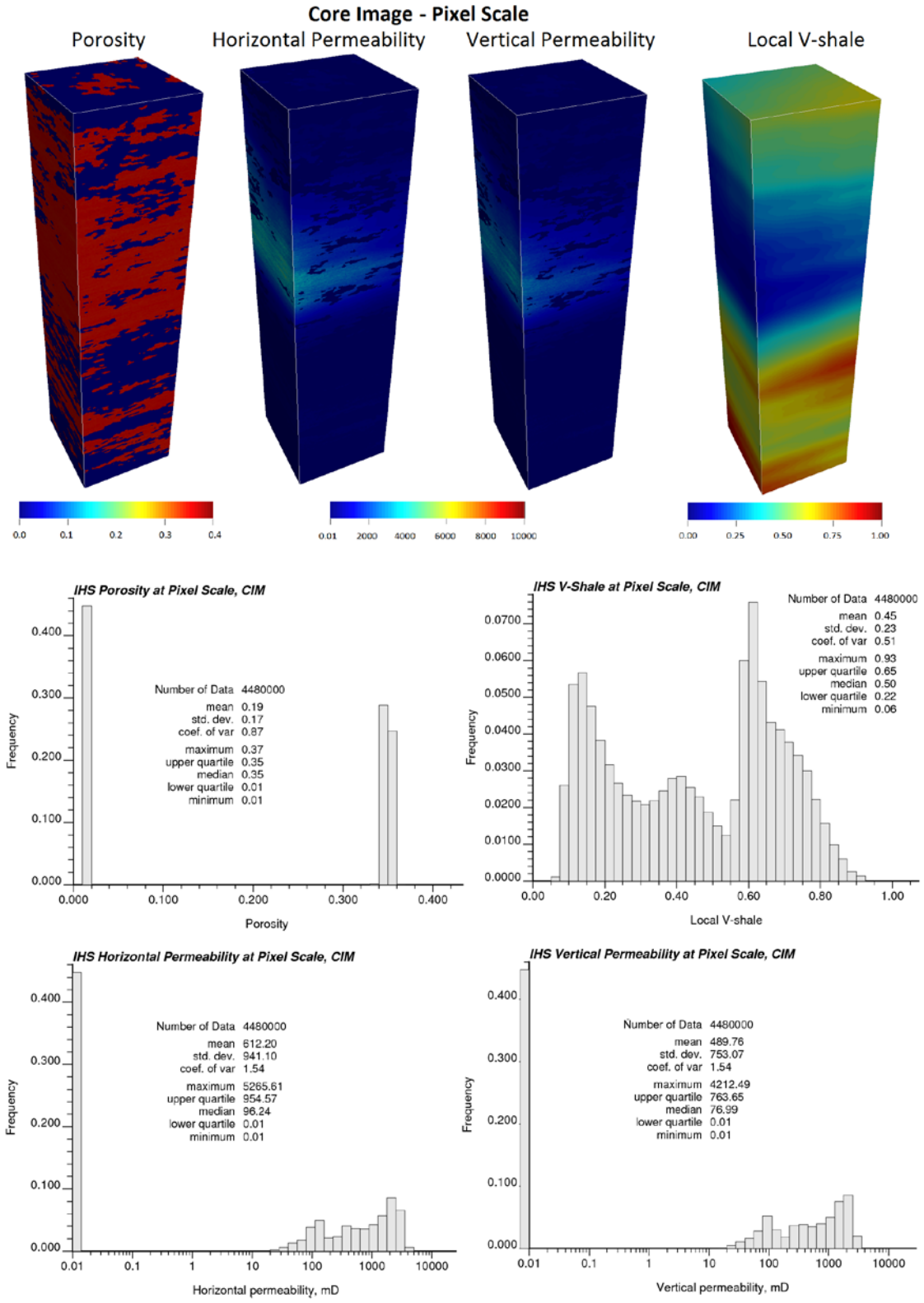

Figure 7: Micromodeling step 6: population of a 3D binary core image-based model with representative clean sand porosity and horizontal permeability values. The model grid consists of 80 x 80 x 700 blocks. The size of single regular block is 0.625 x 0.625 x 0.286 mm^3 and is the same as CIM data resolution.

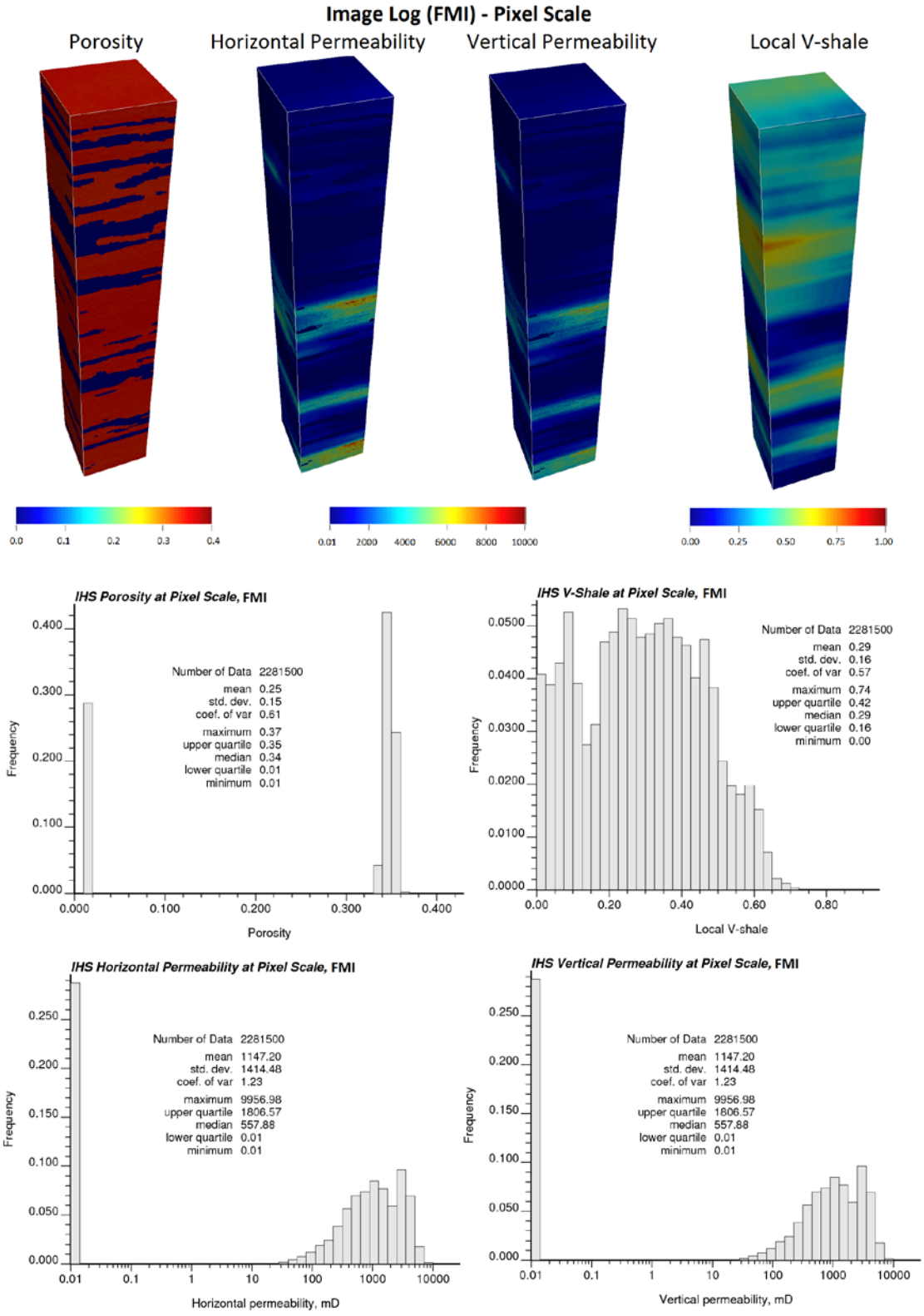

Figure 8: Micromodeling step 6: population of a 3D binary image log-based model with representative clean sand porosity and horizontal permeability values. The model grid consists of 78 x 78 x 375 blocks. The size of single regular block is 2.08 x 2.08 x 2.50 mm^3 and is the same as FMI data resolution.

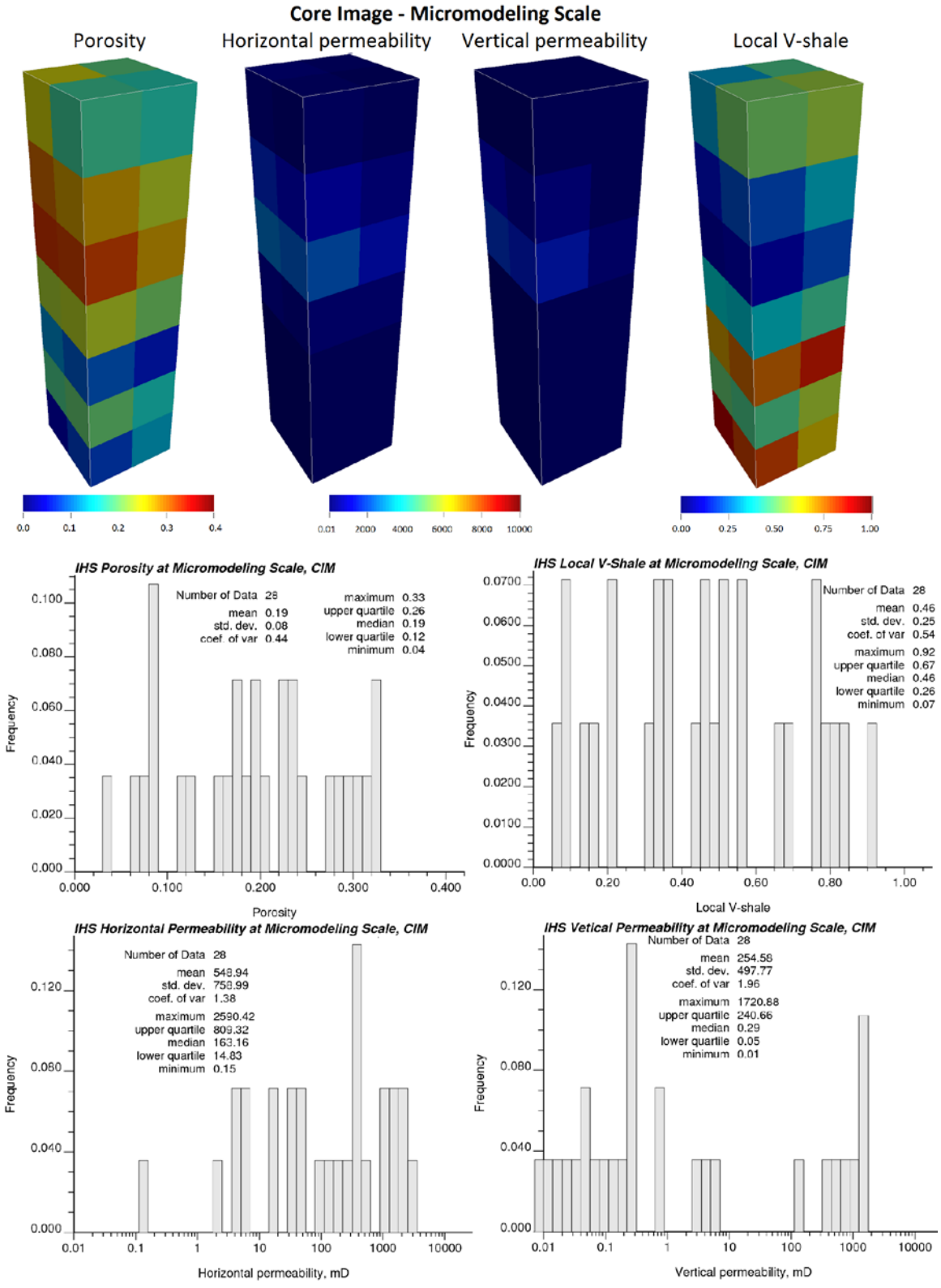

Figure 9: Micromodeling step 7: upscaling properties of populated core image-based model – arithmetic upscaling of porosity and local V-shale, and tensor-based flow upscaling of permeability. The upscaled model grid is 2 x 2 x 7, a block of which has size of 25.0 x 25.0 x 28.6 mm^3.

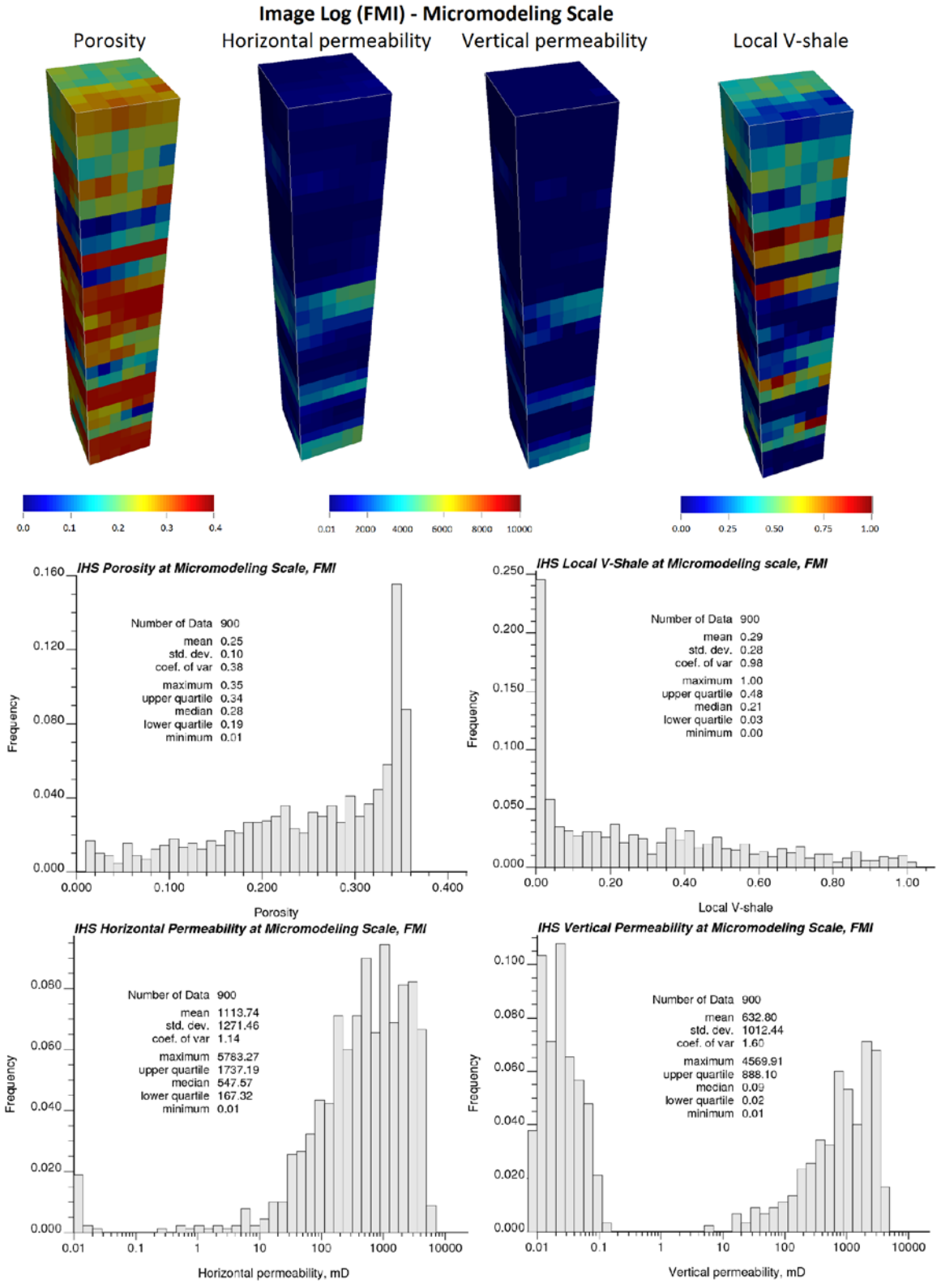

Figure 10: Micromodeling step 7: upscaling properties of populated image log-based model – arithmetic upscaling of porosity and local V-shale, and tensor-based flow upscaling of permeability. The upscaled model grid is 6 x 6 x 25, a block of which has size of 27.04 x 27.04 x 37.5 mm^3.

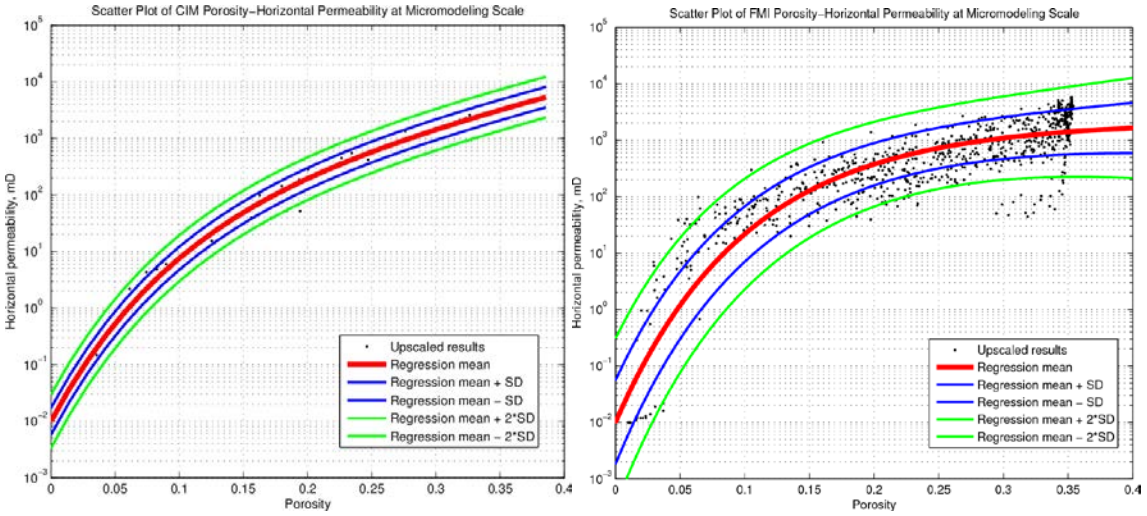

Figure 11: Micromodeling step 8: parametric regression fitting of porosity-horizontal permeability relationship at micromodeling scale of the core image- and image log-based models. FMI-based results have higher uncertainty due to lower resolution of the image and larger model size, thereof, more samples.

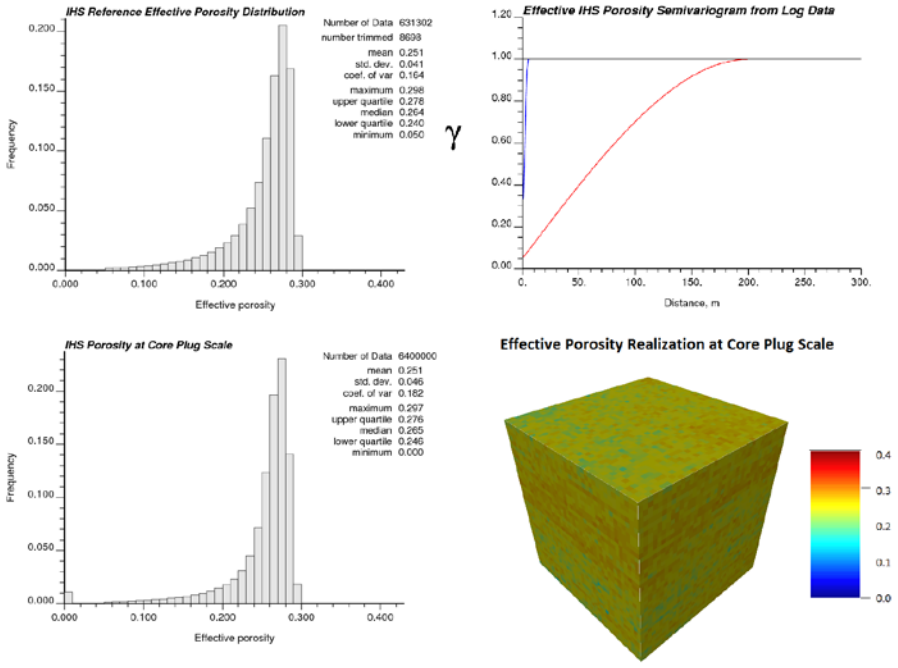

Figure 12: Minimodeling step 1: porosity simulation at core plug scale. Cleaned log porosity data is used as a reference distribution and also to derive variogram model. Note the same porosity model of N = 89 realizations is used for both core image- and image log-based modeling. The grid of core plug scale model is 40 x 40 x 40, and block size is 0.025 x 0.025 x 0.025 m^3. Single realization is shown in 3D. The lamination of IHS structure is slightly reproduced in the 3D model, and could be improved by having real data.

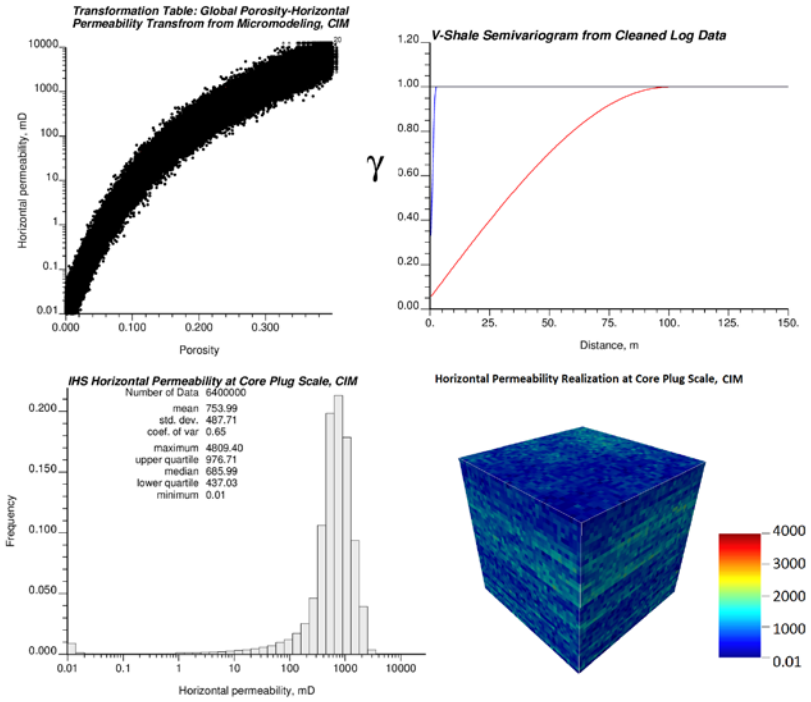

Figure 13: Minimodeling step 2: p-field simulation of horizontal permeability at core plug scale for core image-based model. Bivariate relationship from micromodeling and log V-shale variogram are used in co-simulation. The grid of core plug scale model is 40 x 40 x 40, and block size is 0.025 x 0.025 x 0.025 m^3. Single realization is shown, and IHS lamination is reproduced.

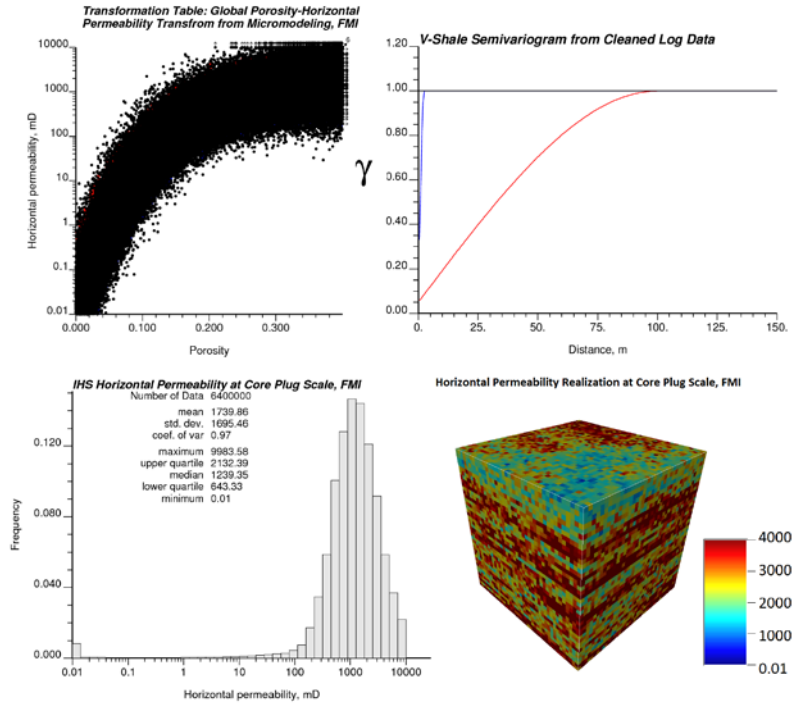

Figure 14: Minimodeling step 2: p-field simulation of horizontal permeability at core plug scale for image log-based model. Bivariate relationship from micromodeling and log V-shale variogram are used in co-simulation. The grid of core plug scale model is 40 x 40 x 40, and block size is 0.025 x 0.025 x 0.025 m^3. Single realization is shown, and IHS lamination is reproduced.

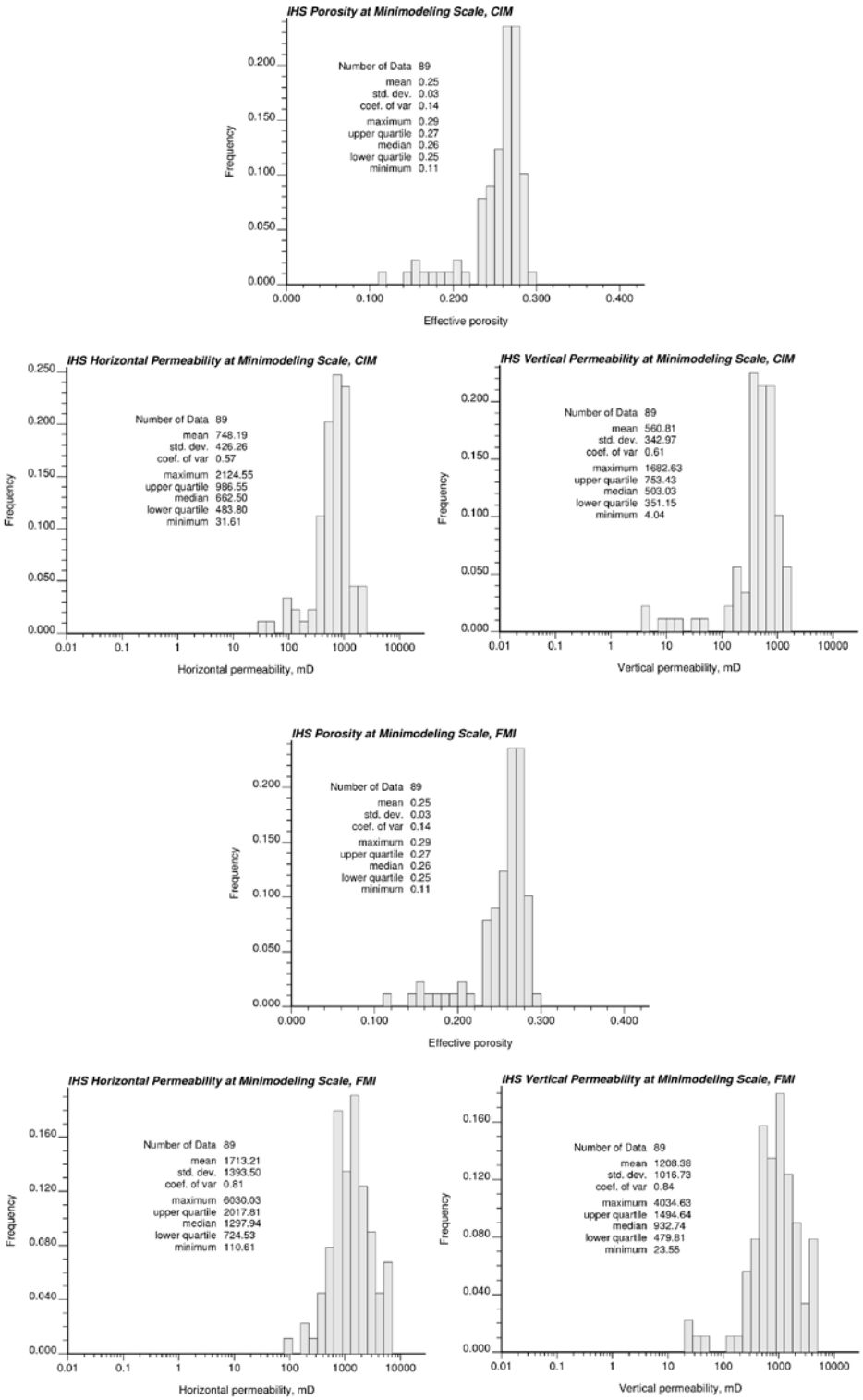

Figure 15: Minimodeling step 3: upscaling properties of populated core image- and image log-based models – arithmetic upscaling of effective porosity and tensor-based upscaling of permeability at minimodeling scale. The mini model grid is 1 x 1 x 1, block size of which is 1.0 x 1.0 x 1.0 m^3. Eighty nine realizations are generated (N = 89). Permeability from FMI is higher than permeability from CIM due to higher shale content in the interval captured by FMI and its less ability to capture smaller scale heterogeneities.

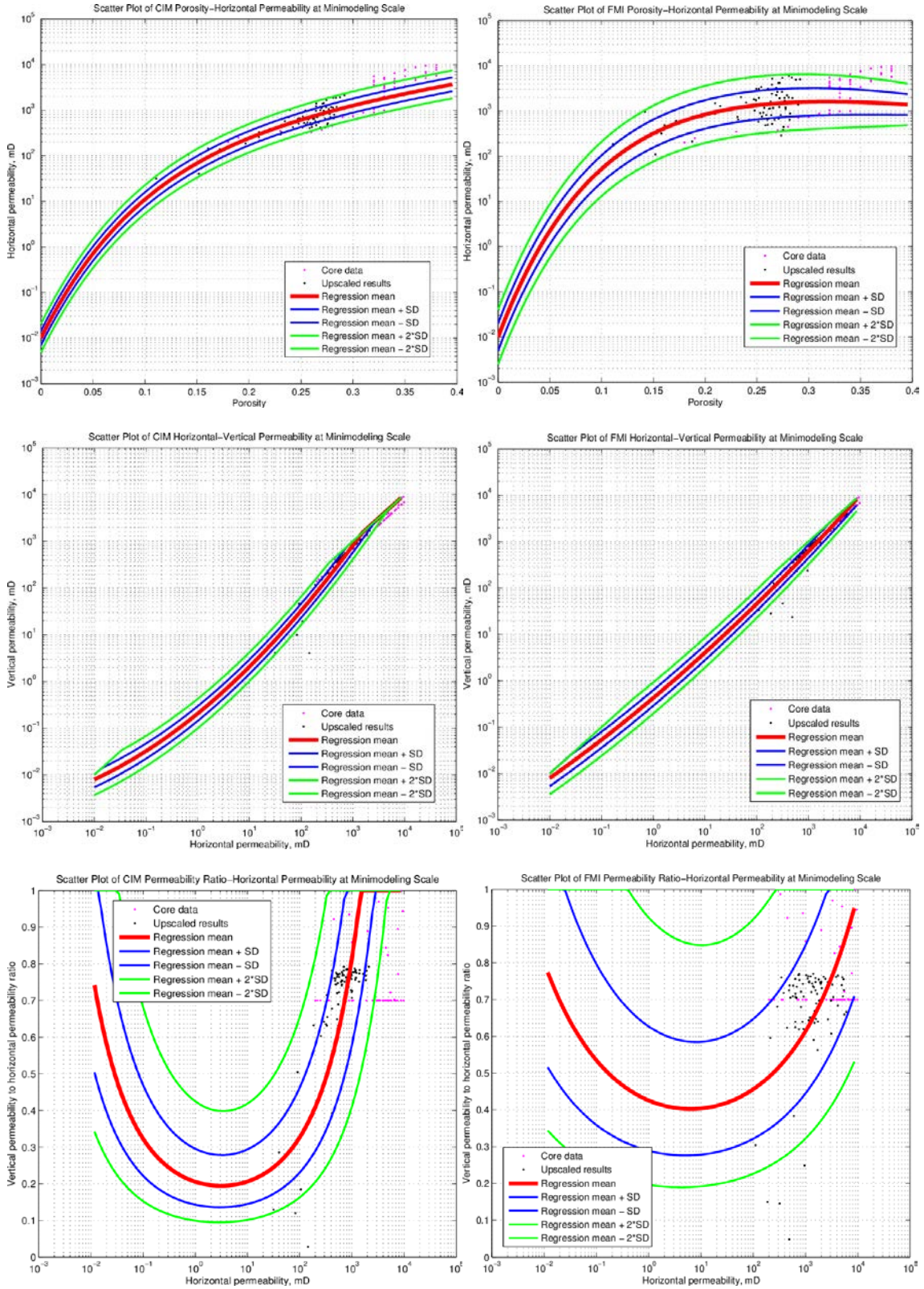

Figure 16: Minimodeling step 4: parametric regression fitting at minimodeling scale of porosity-horizontal permeability and K_{hor}-K_{ver} relationships derived from the core image and image log data. The regression coefficients are stored in Table 4. Values with K_{ver}/K_{hor} ratio lower than 0.3 and higher than 1.0 are not used in the regression fitting. Fictitious core data is debiased by the proposed modeling approach.